Search for New and Unusual Strangeonia in Photoproduction using CLAS

Prospectus of Dissertation

Mukesh Saini

Department of Physics, Florida State University

April 17, 2009

Major Professor	:	Dr. Paul Eugenio, FSU
Committee Member	:	Dr. Dennis Weygand, JLab
Committee Member	:	Dr. Volker Crede, FSU
Committee Member	:	Dr. Simon Capstick, FSU
Committee Member	:	Dr. Tomasz Plewa, FSU
Committee Member	:	Dr. Horst Wahl, FSU

Abstract

We propose to study the strong decay amplitudes, partial widths and production channels of strangeonia from the CLAS g12 dataset obtained during the HyCLAS [1] experiment conducted at Jefferson Lab. The experiment was designed and conducted to search and observe new forms of hadronic matter through photoproduction. HyCLAS was motivated by recent experimental results for gluonic hybrid meson candidates and theoretical Lattice QCD and Flux-tube Model calculations. Crucial among the various channels to be explored in HyCLAS are those for strangeonia, resonances such as $\phi(1680)$ and $\phi_3(1850)$ decaying to $\eta\phi$. This is the signature that will unequivocally identify a strangeonium ($s\bar{s}$) state and will be a main focus of this study. Strangeonia $s\bar{s}$ ($\phi(1680)$ or $\phi(1750)$ or $\phi_3(1850)$) to $\eta\phi$ is an important channel to establish the strangeonia spectrum [2]. $\eta\phi$, $\eta'\phi$ are $s\bar{s}$ signature decay modes due to their negligible interference with non-strange $n\bar{n}$ vector decay modes. $\phi(1020)$ is a $s\bar{s}$ vector meson and the η meson wave-function has a strong component of $s\bar{s}$ in it. Also of interest is the decay channel $\phi\pi^0$ which is an exotic channel due to its OZI suppression. Observation of a resonance decaying to $\phi\pi^0$ would provide a strong evidence of mesons beyond $q\bar{q}$. The data for the proposed analysis comes from the aforementioned HyCLAS experiment. A final state of *proton*, K^+ and K^- will be selected from the dataset. An intermediate ϕ state will be identified by its decay to K^+ K^-. Using energy-momentum conservation, missing mass in an event is calculated. A cut for the missing η or the π^0 mass in their respective mass range will be implemented to identify the missing particle ($\gamma\ p \ \rightarrow\ p\ K^+\ K^-\ [\eta/\pi^0]$). Invariant mass for the ϕ and the missing η/π^0 system will be reconstructed to observe possible resonances. We will study the expected decay channels and widths predicted from various theoretical models and compare them to our experiment wherever possible.

Introduction

Our understanding of strong nuclear force has undergone many major revisions over the last eight decades. Our present understanding of the strong interaction is that it is described by the non-Abelian gauge-field theory of Quantum ChromoDynamics (QCD) [3] [4] [5] which models the interactions of quarks and gluons. Strong interactions are held responsible for binding the quarks within a nucleon and the nucleons within a nucleus. This interquark force is mediated by a fundamental particle called gluon. It is a massless vector boson and carries color charge, analogous to the electric charge. The color charge allows a gluon to self-interact making QCD much harder to solve compared to Quantum ElectroDynamics (QED). Only colorless combinations of elementary particles are physically allowed to exist in nature. This phenomena is referred to as 'color confinement' and it gives rise to our observed world of mesons and baryons.

In strong interactions, we observe no free quarks or gluons. Majority of the scientific community in the 60's believed quarks to be fictitious mathematical devices with almost no physical significance and hence unobserved. The status-quo changed in 1968. In an electron-proton scattering experiment at SLAC, the electrons appeared to be bouncing off small dense objects inside the proton. Bjorken and Feynman analysed this data in terms of a model where a proton was formed of constituent particles though they did not yet refer to the constituents as 'Quarks' but as 'Partons' [6]. This was the first experimental observation of quarks. Whereas in theory, with the discovery of asymptotically free gauge theory in the 70's the whole of theoretical nuclear physics was revolutionalised. This laid the basis for the Standard Model of Particle Physics. Asymptotic freedom also presented us with the idea of confinement. Unlike QED, force between colored charges does not decrease with increasing distance, leading us to believe that the quarks and gluons can never be liberated from an hadron.

Currently we treat QCD in two extreme regimes. First being the perturbative regime where quark interactions have large momenta, hence they are high energy, small distance interactions where the quarks are treated as effectively free. Because the strong coupling constant at short distances becomes much smaller than 1 ($\alpha_s < 1$), perturbative expansions in α_s are valid. QCD has been reasonably successful in this region. Second is the non-perturbative regime where quarks and gluons are tightly bound within a hadron, so QCD becomes non-linear and we have to resort to specific hadronic models. Alternatively, there are ongoing efforts to solve QCD on a Lattice [7]. While Lattice QCD has made great advances within the last decade, it will be several more years before Lattice QCD results confront the experimental data [8].

Meson physics and strong interactions have been intricately connected ever since 1935, when Yukawa first introduced pions [9] to explain the internucleon force. Mesons make for ideal studies of strong interactions in the strongly coupled non-perturbative regime in order to understand QCD [10] [11]. Every physical meson state spans over a basis of $\{\ |q\bar{q}\rangle \quad |q\bar{q}g\rangle \quad |gg\rangle \quad |q\bar{q}\rangle^2 \ \ldots\}$ states. The amplitudes of the basis expansion for a meson are determined naturally by QCD interactions. We conveniently 'classify' a state as a meson, hybrid, glueball or something else depending on the most prominent state in the basis expansion for the resonance.

Motivation

Constituent Quark Models picture a nucleon as a color neutral set of three valence quark flavors as the ones determining the nature of the nucleon. Hitherto with the meson. An exotic meson is a resonance with J^{PC} or other quantum number forbidden to $|q\bar{q}\rangle$ states of non-relativistic or conventional quark model [2] [12] [13]. A Quick Overview: In the constituent quark model, conventional mesons are bound states of a spin $\frac{1}{2}$ quark and a spin $\frac{1}{2}$ antiquark. The quark and antiquark spins combine into a spin singlet or triplet state with total spin $S = 0$ or 1 respectively. S is coupled to the orbital angular momentum L to give total angular momentum $J = L$ for the singlet state and $J = L-1,\ L,\ L+1$ for the triplet states. In spectroscopic notation the resulting state is denoted by $n^{2S+1}L_J$ where n is analogous to Principal quantum number, with S for $L = 0$, P for $L = 1$, D for $L = 2$, and so on. Parity is given by $P(q\bar{q}, L) = (-1)^{L+1}$ and C-Parity is also defined for neutral self-conjugate mesons and is given by $C(q\bar{q}, L, S) = (-1)^{L+S}$. For example, the lowest state for a vector meson with $J^{PC} = 1^{--}$ is the 1^3S_1 quark model state. In case of the members of an isospin triple there is another quantum number, G-parity, which is defined as $G \equiv C_n(-1)^I = \pm 1$ and has the same value for all members of the triplet, where C_n is the C-parity of the neutral member. G-parity is a near exact symmetry of strong interaction for light quarks because of the inherent approximate nature of isospin for the light quarks [12].

An exotic meson is defined as a state orthogonal to $|q\bar{q}\rangle$ states of the non-relativistic quark model. An exotic can possess J^{PC} spin parity or other quantum numbers forbidden to quark model resonances [13]. A gluonic hybrid meson is a resonance for which the dominant component in the basis expansion is $|q\bar{q}g\rangle$. In principle, gluonic hybrid mesons are able to have all possible J^{PC} states including those which are not accessible to the conventional $|q\bar{q}\rangle$ meson state. If we are to observe and identify any exotica, hybrid meson spectra needs to be studied and documented carefully. This will help us distinguish between the two spectra. A certain amount of configuration mixing naturally occurs between these states. Hybrid states with J^{PC} quantum numbers inaccessible to $q\bar{q}$ states are called spin-parity exotics [14].

$$\mathrm{J}^{PC}\Big|_{exotic} = 0^{--}, 0^{+-}, 1^{-+}, 2^{+-}, 3^{-+}, \ldots \; .$$

Since gluons carry color charge and hence self-interact, they are predicted to form quark free-color neutral states called glueballs. For baryons there are no J^P exotics and a hybrid baryon resonance would be observed by an overpopulation of experimental baryon states relative to the qqq spectrum. Two current popular models for Hybrids are the MIT bag model & Flux-tube Model. These models have a specific interpretation for their "excited glue" component [13] [14] [15] [16].

Bag Model: MIT Bag Model treats quarks and gluons as spherical cavity modes of Dirac and Maxwell quanta, confined within the cavity by the choice of color boundary conditions. The zeroth-order states are $\{\ |q\bar{q}\rangle \quad |q\bar{q}g\rangle \quad |gg\rangle \quad |q\bar{q}\rangle^2 \quad . \; . \; .\}$. These bare basis states are mixed by quark-gluon and gluon self interactions to give physical states. In the bag model the lowest quark mode is a $J^P = 1/2^-$ mode while the lowest gluon mode is $J^P = 1^+$. Combining these lowest lying modes, we obtain hybrid basis states with the following spin-parity quantum numbers:

$$\mathrm{J}^{PC}\Big|_{\text{bag model}} = (0^-, 1^-) \otimes 1^+ = 1^{--}, 0^{-+}, 1^{-+}, 2^{-+} \ .$$

Lattice QCD: In Lattice QCD, space-time is treated as a grid created of discrete points/vertices which are joined by lines. A quark can be located at any point whereas a gluon can only travel along the lines joining these points. So in LQCD, the space-time is in effect treated as a crsytal lattice of a lattice spacing 'a'. As the Lattice spacing is decreased, we move towards a more realistic description of QCD. LQCD is computationally very intensive and has been making progress towards giving a more realistic description consistent with the experiments [7] [8].

Flux-tube Model: The flux-tube model is a Lattice QCD inspired description of combined gluonic degrees of freedom with quark degrees of freedom. In Lattice Gauge Theory simulations, a roughly cylindrical region of chaotic glue fields is observed between widely separated static color sources. This "flux-tube" can be excited contributing to the dynamics of the system. Flux-tube is the origin of the confining linear potential between the $q\bar{q}$ meson color singlet, familiar from the quark potential models. An excited flux-tube's orbital angular momentum when combined with the $q\bar{q}$ spin and angular momentum gives us the flux-tube hybrid spectra,

$$\mathrm{J}^{PC}\Bigg|_{\text{flux-tube hybrids}} = (0^{-+}, 1^{--}) \otimes (1^{+-}, 1^{-+}) = 0^{-+}, \underline{0^{+-}}, 1^{--}, \underline{1^{-+}}, 1^{+-}, 1^{++}, 2^{-+}, \underline{2^{+-}} \ .$$

Note: The underlined J^{PC}'s are exotics and not allowed for conventional $q\bar{q}$ states. We are looking to identify the discrepancies between the observed meson spectrum and and the conventional quark model predictions which may signal new physics beyond conventional hadron spectroscopy.

Strangeonia

Strangeonia are unflavored $s\bar{s}$ mesons primarily associated with the excited radial and orbital states of the ground state $s\bar{s}$. The study of strangeonium states can serve as a bridge between short and large distance behavior of the QCD confinement potential because of the intermediate mass of the strange quarks between light mesons and the charmonium sector. Excitations of $s\bar{s}$

provide a range of quark separations, where the confinement potential can be studied from the perturbative to the non-perturbative regime (from high momentum q^2 to Low momentum q^2 transfer). Understanding of the $s\bar{s}$ spectrum will help us bridge the gap between Heavy Quark Effective Theory and the abundant light quarks around us. Of the 22 expected strangeonia below 2.2 GeV, only 7 probable resonances - $\eta\ \eta'$, $\phi(1020)$, $h_1(1386)$, $f_1(1426)$, $f_2'(1525)$, $\phi(1680)$ and $\phi_3(1854)$ are well identified where we count the maximally mixed $\eta\ \eta'$ as one resonance [2]. Of these, the $h_1(1386)$ still needs additional confirmation.

Photoproduction of mesons occur primarily through Vector Meson Dominance where a photon becomes a $q\bar{q}$ pair conserving its spin parity $J^P = 1^-$. Hence we consider the vector photon as a vector meson (ρ, ω, ϕ) with a high content of $s\bar{s}$ and we expect to observe a radial excitation $\phi(1680)$ of the ground state $s\bar{s}$ vector meson $\phi(1020)$. This state has been observed in e^+e^- production and disputed in Photoproduction [19] [18].

Past photoproduction experiments have observed the mass of a resonance near 1750 MeV/c^2 as an enhancement in the mass of K^+K^- [17]. Majority of the experiments suffered from low statistics with about few hundred events at best. These experiments also assumed that any observed state was a diffractively photoproduced vector meson. Hence an observation near 1750 MeV/c^2 was identified with the $\phi(1680)$ from the e^+e^- experiments [18]. In e^+e^- production the $\phi(1680)$ mass averages nearer to 1680 MeV/c^2 while in photoproduction the mass for the same (assumed) resonance is closer to 1750 MeV/c^2. It was originally thought that these observations were of the same resonance with the mass shift due to interference effects with other decay channels. The FOCUS experiment at Fermilab recently claimed that the structure in photoproduction at 1750 MeV/c^2 is a different resonance [19]. The $\phi(1680)$ resonance has been clearly established in e^+e^- production with the dominant decay channel being KK^* ($e^+e^- \to K_sK\pi$). Meanwhile FOCUS measured the $\phi(1750)/X(1750)$ mass to be 1753 MeV/c^2 with its dominant decay mode being K^+K^-. FOCUS found no photoproduced enhancement in the sample for KK^* corresponding to the 1750 MeV/c^2 state in K^+K^-. They state that interference effects could be possible but an unlikely reason for this resonance and they claim $\phi(1750)$ to be a new state, different from the $\phi(1680)$.

The $\phi(1680)$ resonance either behaves differently based on its production mechanism or its an altogather different resonance [19]. This issue is still an open question. The FOCUS observation is cited under and included with the $\phi(1680)$ in PDG and is not as of yet listed as a seperate state [18]. Recently, it was proposed that a structure observed at 2175 MeV by the Babar Collaboration is a 1^{--} strangeonium hybrid [20] [21]. Also open to being observed in our dataset is the possibily of $\phi_3(1850)$ resonance claimed to have been seen in earlier experiments, though these resonances are at the edge of our observational range.

Proposed Analysis

I propose to analyse the data obtained from our g12 run-period to study the final state $\gamma p \rightarrow pK^+K^-[X]$ where an additional neutral particle such as π^0, η or a possible ω will be identified by energy momentum conservation. Identifying an intermediate ϕ meson will allow access to study the $\phi\eta$, $\phi\pi^0$ and possible $\phi\omega$ states. Of these, the $\phi\eta$ channel can only arise from an initial $s\bar{s}$ state in accordance with Zweig rule and thus is free from interference effects with $n\bar{n}$ ($u\bar{u}$ + $d\bar{d}$) states. Hence, our analysis should be able to help clarify the issue of $\phi(1680)/\phi(1750)$ further.

For the $\phi\eta$ system, we will analyse the channel $\gamma p \rightarrow pK^+K^-[\eta]$, where we expect the proton to act as a spectator in a low momentum transfer, low t channel reaction. Final state of *proton*, K^+ and K^- will be selected and an intermediate ϕ state identified by selecting on the invariant mass of the K^+ K^- system. Using energy-momentum conservation, a missing eta will be identified and the invariant mass for the ϕ and the missing η system will be reconstructed to observe possible resonances. Similar techniques will also be used to look for other decays in various channels like the exotic $\gamma p \rightarrow pK^+K^-[\pi^0]$ and $\gamma p \rightarrow pK^+K^-[\omega]$. Both $\phi\pi^0$ & $\phi\omega$ channels are exotic as they are OZI suppressed decays for $q\bar{q}$ mesons [22] [23].

The Experiment

The dataset for this analysis comes from the g12 experiment conducted at Jefferson Lab, Newport News, Virginia. The experiment took data from April 1, 2008 to June 9, 2009 over 70 calendar days and acquired 26.2 *billion* triggers (events of interest). This amounts to 68 pb^{-1} of physics data which is spread over 63010 raw data files, each of $\sim$ $2GB$ and occupies $\sim$ 126 TB of memory space on tape. After processing, the raw data can expand by a factor of 6. Our experimental data was taken in Hall-B using the CLAS detector [24]. CLAS has an almost 4π solid-angular coverage. The beam to the detector was provided by CEBAF (see Figure 1). CEBAF delivers continuous electron beam to Hall-B of energies up to 5.7 GeV with electron beam current ranging between 2-90 nA which turns out to be optimum for CLAS. Our data run 'g12' took most of its production data in the 60-65 nA range. This electron beam was incident on a radiator to provide CLAS with a photon beam. This beam has a 2.004 ns bunch structures.

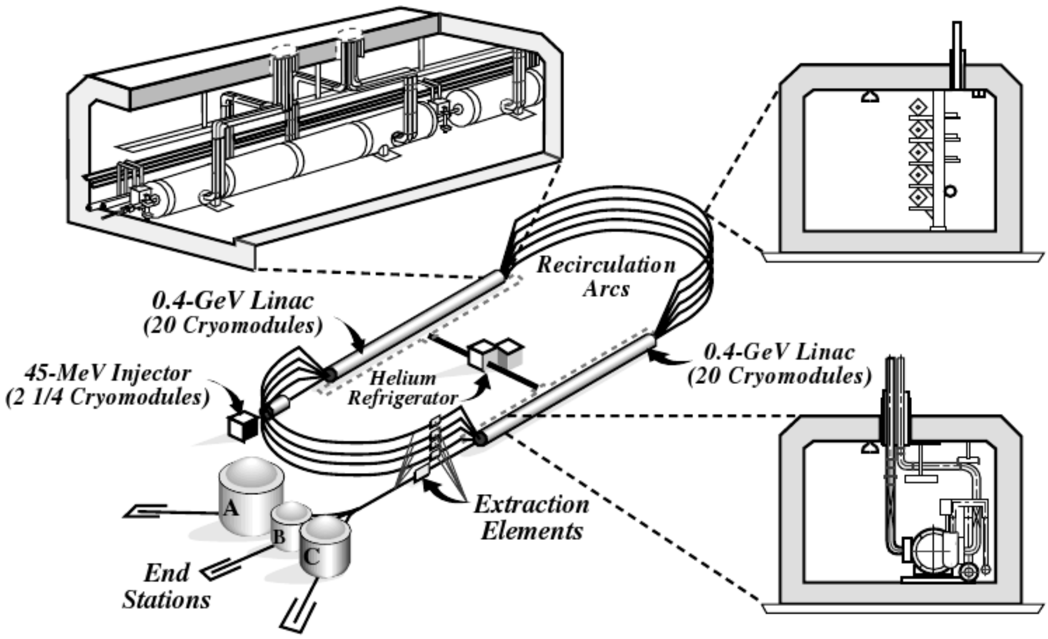

Figure 1: Schematic layout for CEBAF. Shown are the 5-pass recirculation arcs and the two linacs composed of cryomodules. A 5-pass electron beam can be extracted and delivered to the end-stations - Halls A,B,C.

CEBAF, the Continuous Electron Beam Accelerator Facility (See Figure 1), is located at the Thomas Jefferson National Accelerator Facility in Newport news, Virginia [24]. CEBAF delivers a high intensity continuous electron beam in an energy ranging from 0.8 GeV to 6

GeV and operating current between 2 nA - 100 μA to the individual halls. Electrons are pre-accelerated before being injected into the north linac. Each pass through one of the linac's gives it an energy boost of ≈ 0.6 GeV. Due to the continuous nature of the electron beam produced, multiple beam energies are simultaneously present in each linac. A beam can make a maximum of 5 passes and can be polarised linearly or in a circular manner as per the requirement. At the South linac, these beams are extracted and given to the three experimental halls with energies in multiples of ≈ 1.2 GeV.

For the g12 experiment, 5.71 GeV electron beam was delivered to Hall-B from CEBAF. The electron beam was then incident on a radiator to produce a hight energy photon beam. The electrons were removed from the beamline with the Tagger magnet, which bends the scattered electrons towards the tagger assembly and the non-interacting beam to a dump. Using energy conservation and the geometry map for the magnetic field, the energy and the time for a photon reaching the detector corresponding to an electron in the tagger is calculated. Thus tagger magnetic spectrometer provides photons tagged with their energy and time of interaction for further data analysis in the CLAS. Our main experimental trigger was set up to accept two or more charged tracks in the CLAS where the tagged beam photon energy was ≥ 4.4 GeV. This corresponded to selecting a hit in the first 25 scintillators of the tagger based on the geometry of the tagger magnetic field in use.

CEBAF Large Acceptance Spectrometer (CLAS) is divided into six sectors by a super-conducting, toroidal magnet (See Figure 2). Each of these sectors serve as an independent spectrometer. Immediately surrounding the target area is a start counter (ST) composed of 24 scintillators. The purpose of the start counter is to provide a time stamp for the start of an interaction so as to match this time to a certain tagged beam photon. Moving from the inside of CLAS to the outside, after the ST are the Drift Chambers (DC). DC is divided into 3 regions in each of the six sectors by CLAS toroidal magnets. where *region* 1 lies in a low magnetic field, *region* 2 lies in a high magnetic field and *region* 3 has no magnetic file. This setup helps us in determining the momentum of a charged particle traversing the CLAS. Following the DC, there is another set of scintillators called the time-of-flight (TOF) scintillators. The TOF provides

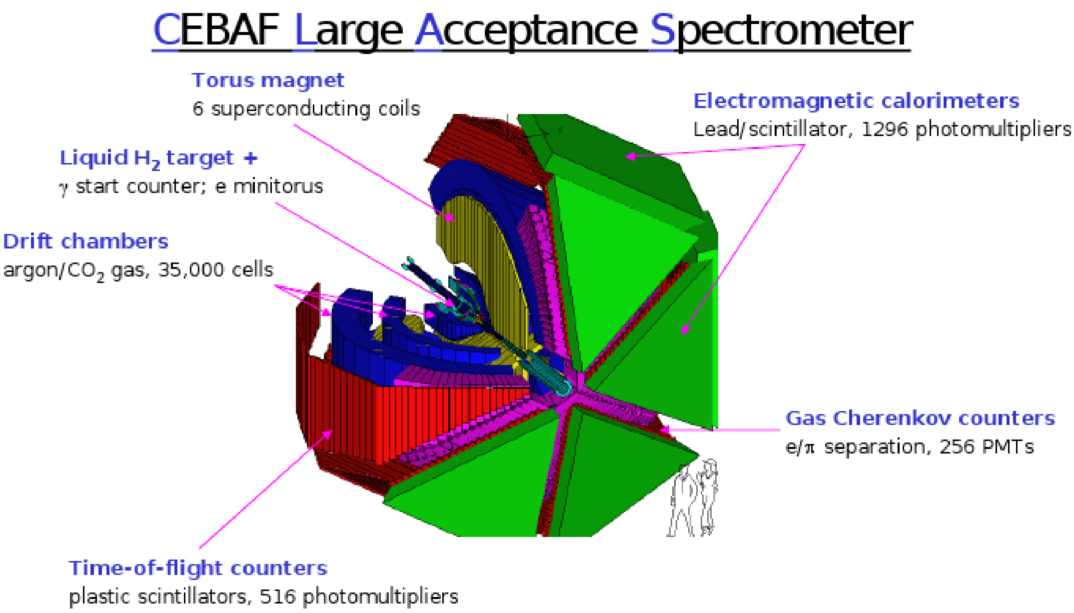

Figure 2: CLAS detector and its components are labeled. Each sector is an independent spectrometer consisting of the Target Cell, Start Counter for γ runs, 3 Drift Chamber regions (blue), Torus magnet (yellow), TOF (red), Cherenkov counters (pink) and the electromagnetic calorimeters (green).

timing information to be used with the particle tracks and the start counter in order to find the velocities and energies of the outgoing particles. This information is used along with the information about momentum from the DC to calculate the mass of each particle in CLAS and thus provides particle identification. In the forward region of CLAS are the electromagnetic calorimeters and Cherenkov detectors primarily used for the detection of electrons. The target is generally placed at the center of CLAS. In our experiment though it was placed at 90 cm upstream of the center of CLAS. This was done to increase the forward angular coverage of CLAS for better observing peripheral meson production. All the subsystems are designed to follow and maximise the benefits of the sector based geometry of CLAS.

After data taking, the CLAS detector must be calibrated to determine and account for run by run variations in detector operations. These variations occur because of changes in environmental factors and detector performance. These calibrations take a long time and require multiple iterations. Many people are dedicated to this process and progress has been slow and steady.

After satisfactory calibrations of all the detector components, we start data and physics

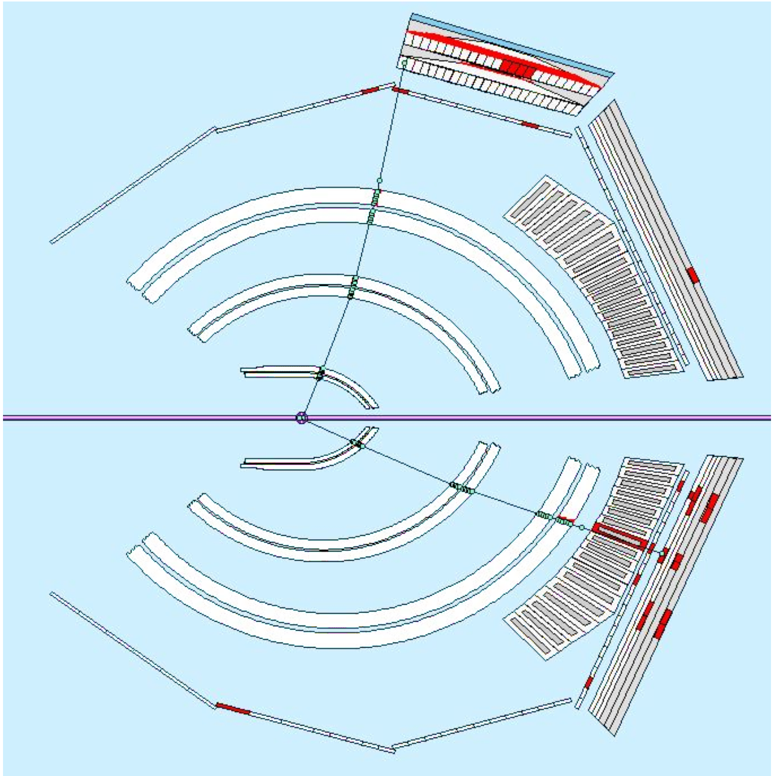

Figure 3: Example of tracking in CLAS as shown by the CLAS Event Display (ced). Tracks are reconstructed from the hits highlighted in the various detector components (ST, DC, TOF, EC, CC for tracks on display). Curvature of the track implies that the particles are charged and helps determine the momentum of the particle.

reconstruction from the CLAS raw data which consists of signal information from thousands of PMT's, ADC's, TDC's and other electronic components. Detector hits are reconstructed from hits in the DC to form particle trajectories (tracks). See Figure 3. Thus we obtain the timing of the hit, path, pathlength, momenta and other information used to conduct particle identification. The final output of this is a data file which contains the information about reconstructed event tracks, timings, particle id, energy, momentum and other physics information in it.

We monitor these output data files for the quality of our data and calibrations. Other new customised packages have been developed to monitor the data quality for the whole run-period too. We expect to go to the first pass by the end of June after we make sure that all the calibrations are stable and major issues resolved. Data analysis will be done in parallel and skims generated. Hopefully there will be some results to present, maybe even publish by the end of next year.

Calibrations

As part of my contribution to the experiment and the collaboration, I am responsible for calibrating the tagger spectrometer as well as the start counter for the g12 experiment. A brief synopsis of those efforts follows.

Tagger Calibrations

The tagger magnetic spectrometer provides photons tagged with their energy and time of interaction for further data analysis. CLAS tagger is composed of 61 timing scintillators (T-counters), which can be divided into 121 T-bins due to the overlaps between two counters. Each scintillator is equipped with two photomultiplier tubes (left and right), and the signal is treated by constant fraction discriminator. In addition, there are 384 narrow overlapping scintillators covering the same range, used for the energy determination divided into 767 energy bins. Each energy counter (E-counter) is equipped with one PMT. In addition to photon energy determination, the aim of the tagger analysis is to substitute the reconstructed tagger time for an event with its proper accelerator RF time, the most accurate clock in CLAS. This is crucial since CEBAF accelerator electron bunches are separated by 2.004 ns. An error of one RF bunch in the tagger calibration will propagate to the particle ID and compromise our ability to identify the correct beam photon and distinguish pions from kaons.

The relative timing between T counters must be aligned in order to obtain an overall tagger time resolution which allows to discriminate unambiguously between two RF buckets (2 ns apart). The time of the beam photon is measured by the CLAS Bremsstrahlung tagging system (Tagger) and then corrected for the phase difference between the tagger time and the RF time. After this alignment, the RF time is assigned to the photon which is then propagated the event vertex to give the interaction time for the event.

Calibrating the tagger involves calibrating to the accelerator RF timing. For the tagger calibrations parameters are determined for the TDC slopes (2 x 61 for left and right), base peak positions (2 x 61 constants for left and right T counters, 384 constants for E counters), RF fine adjustment constants (121 constants for each T-bin), overall tagger time offset with

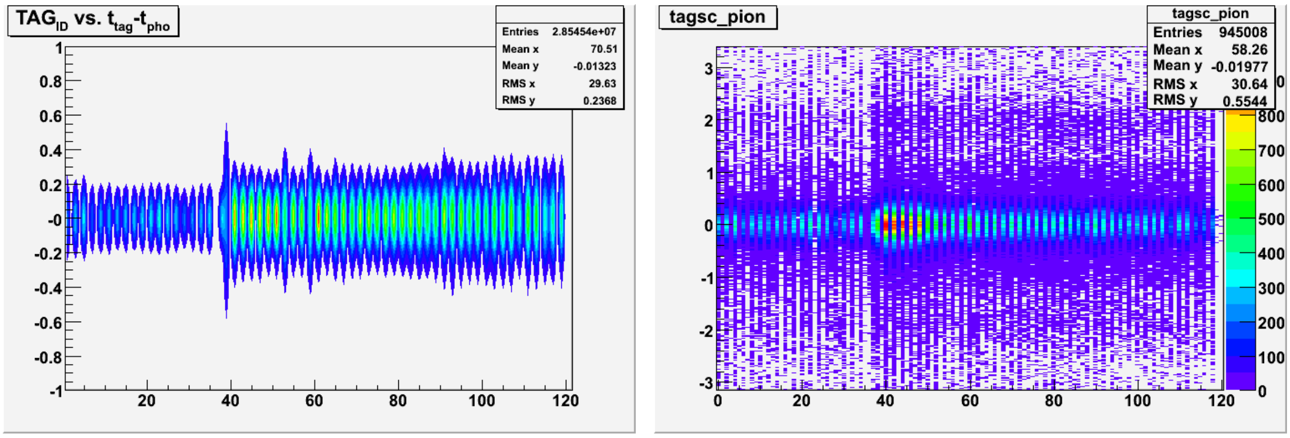

(a) RF & Tagger T-Counter alignment within the RF bucket

(b) Overall alignment of the 121 Tagger T-Counters with the RF beam buckets

Figure 4: 2D calibrations plots used for tagger T-Counter alignment. Each bin is a T-counter that has been calibrated to the RF. The alignment of the distribution of each bin around zero indicates a good calibration.

respect to CLAS detectors (TOF $\rightarrow$ tag2tof, Start Counter $\rightarrow$ st2tof,..) (1 constant each). Figure 4 shows the proper alignment of the tagger T-counters within a RF cycle (Figure 4a) as well as with respect to each other (Figure 4b).

Start Counter Calibrations

Start counter is the closest detector subsystem to the target. Hence it serves as the best source to identify the start time of an event. It was also used in the Data-acquisition trigger logic to identify and acquire the interactions of interest.

The start counter is a hexagonal shaped cylindrical scintillating barrel with a cone shaped nose (See Figure 5). It is constructed of 24 scintillator paddles with phototubes connected to one of their ends. Start counter surrounds the target reflecting the sector-wise structure of CLAS. It has six sectors, each sector comprising of 4 scintillator paddles. The scintillating paddle has a rectangular region: 2.15 mm thick, 29 mm wide and 502 mm long. There is a bend near the phototube end for light guide coupling and a bend at the down stream end forming a piece of the nose. The start counter was designed to provide full acceptance coverage defined by the CLAS detector with a 40 cm long liquid hydrogen target.

The main technique for particle identification in CLAS is through the measurement of

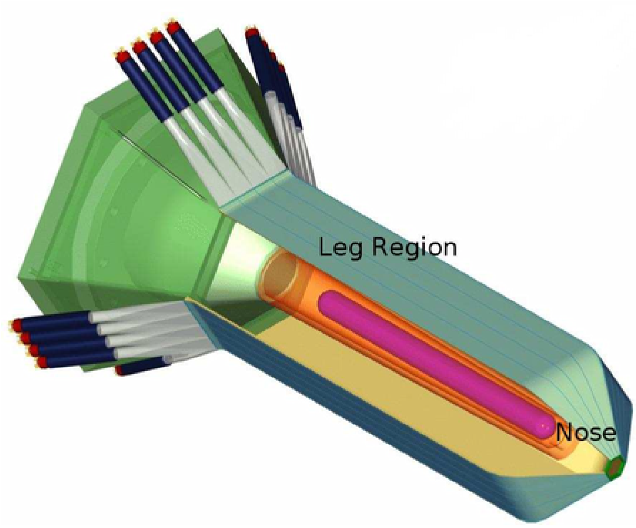

Figure 5: Sketch of the CLAS start counter depicting the 6 sector, 24 scintillator arrangement. Shown are the phototubes upstream connected by light guides to the scintillator. The downstream end of the ST forms a cone-shaped region called nose with an opening to let the beam through.

the time-of-flight of the scattered particle from the interaction vertex to the outer detectors (TOF or EC). The time of interaction is obtained by determining the photon beam RF time at which the event occurred. For this purpose a sub-nanosecond coincidence of the tagging spectrometer with the start counter close to the target region is used. The time of interaction at the target must be determined to ± 1 ns. For a Gaussian time distribution, this translates into a standard deviation of 388 ps. All start counter paddles have to be calibrated individually and aligned in time. This is done by calibrating the time delay for each paddle to tune the time at which a particle hits the ST paddle. Figure 6a shows the start counter's alignment when I began calibrations and figure 6b shows the start counter's alignment when it has been properly calibrated and aligned. The alignment at zero shows the alignment of the start counter with the accelerator RF cycle. Figure 6b is a good calibration for the start counter.

The calibration constants obtained in the process are: time off-set between paddles, effective velocity in leg region, nose region fit parameter, nose region fit parameter, nose region fit parameter & three time-walk parameters. Thus after calibrations the start counter signal in coincidence with the T-counter time propogated to the target allows for good identification of the photon RF time in coincidence with the hadronic interaction in the target. Comparison to

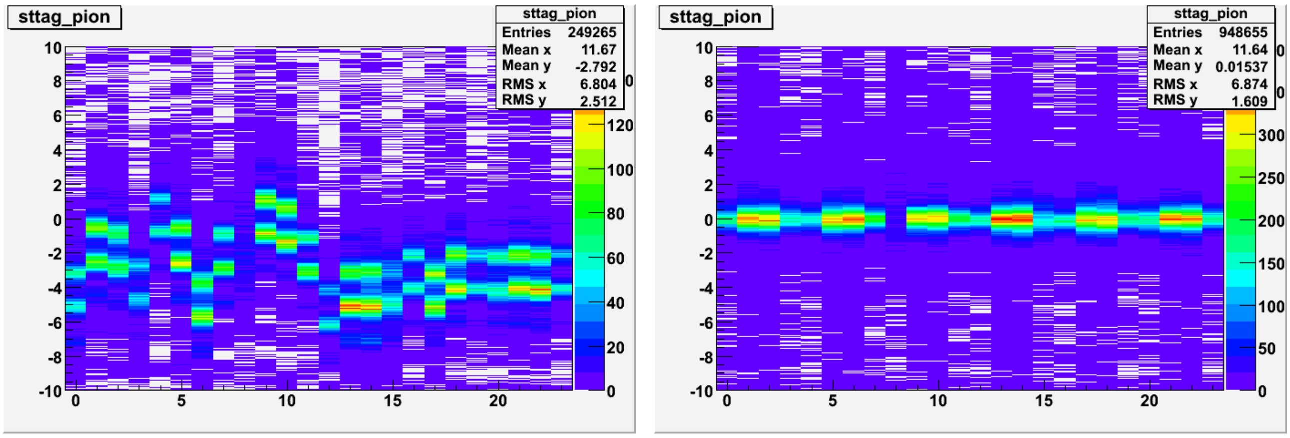

(a) Before

(b) After

Figure 6: 2D calibrations plots for Start Counter paddle to paddle alignment. Each of the 24 bins represents a ST paddle, with the cross-section being the tagger photon time at the vertex subtracted from the start counter vertex time. Figure 6b shows a properly calibrated start counter with all paddles aligned with the RF cycle as well as with each other.

the nearest RF time gives the start time of the particle trajectory to better than 25 ps. For example, an integral part is the time walk correction which corrects for pulse height slewing for individual ADC's of a paddle (See Figure 7). Once all the detectors are aligned with respect to each other, one can extrapolate the start time of the event from the hit position on the start counter to the interaction vertex. Once this is done one can identify the corresponding RF time bucket producing the interaction with a resolution of $\approx$ 460 ps presently.

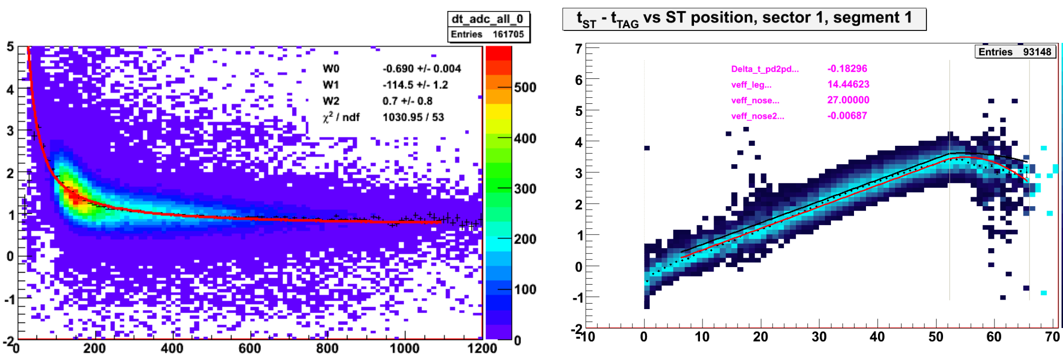

(a) ADC spectra for a ST paddle used for Time-walk correction of ADC signal (dt versus ADC channel)

(b) Reconstructed ST hit time for hit positions on the paddle, used to calibrate the effective velocity of light for a scintillator (dt versus hit position)

Figure 7: Crucial calibrations for start counter timing resolutions.

Particle Identification

Once all the detector subsystems are reasonably calibrated, particles can be identified by their timing. In CLAS charged particle such as pions, protons, kaons are identified by the time of flight mass, which primarily depends on accurate measurements of momentum from DC and time of particles flight from TOF (See Figure 3). In the plot of β versus momentum, one can see the separate bands for pions, protons, kaons like in the Figure 8. Mass of the particle is calculated in the straightforward manner as follow and that completes our initial primary particle identification.

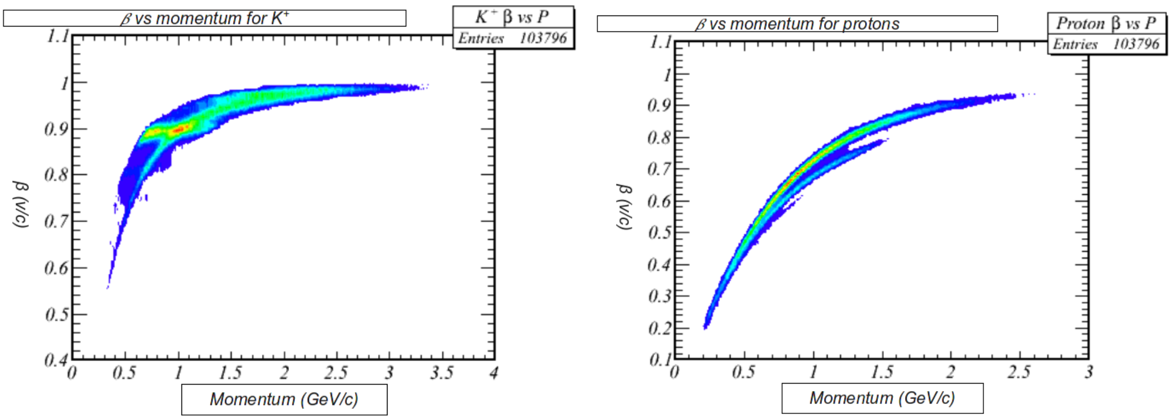

(a) β vs momentum plot for K^+ (b) β vs momentum plot for *protons*

Figure 8: β (v/c) vs Momentum plot for 2 of the the final state particles, K^+ and *proton*. These bands are representative of the particle mass and hence also show any misidentification of particles. Figure (a) for K^+ shows a band of pions misidentified as kaons around $\beta \sim 0.9$.

$$Mass = \frac{P}{\beta.\gamma(\beta)} \tag{1}$$

where momentum comes from drift chambers and β as follows,

$$\beta = \frac{v}{c} = \frac{pathlength\ from\ event\ vertex\ to\ TOF}{Particle's\ flight\ time,\ calculated\ from\ vertex\ to\ TOF\ *\ c} = \frac{l}{\Delta t}.\frac{1}{c} \tag{2}$$

After this initial ID we make further stringent selection cuts on vertex, timings, momentum, energy loss to get a more accurate particle identification.

Preliminary analysis

I will analyse the data obtained from our g12 CLAS run-period to study the final state $\gamma p \rightarrow pK^+K^-[X]$ where an additional neutral particle such as π^0, η or a possible ω will be identified by energy momentum conservation. Identifying an intermediate ϕ meson allows access to study the $\phi\eta$, $\phi\pi^0$ and possible $\phi\omega$ states. Based on preliminary analysis of $\sim 8\%$ of the data, I anticipate an observed yield of about 1000 $\gamma p \rightarrow p\phi\eta$ events from the whole g12 run-period. An attempt was made to study this channel in earlier CLAS data but the analysis was inconclusive due to a lack of statistics [1]. At present, analysis tools are still being developed and processed. Listed below are few of the cuts that will be implemented in the analysis. These cuts will be refined further along the analysis.

Events with at least three charged tracks are selected so as to have an inclusive sample of pK^+K^- events. Only events with beam photon energy greater than 4.4 GeV are selected to remove the low energy events. Cuts are applied on the event vertex to make sure the event originates inside the target. Timing cut on the interaction time (± 1 ns) is applied using the start counter and the RF to ensure that the right photon is selected. In order to identify peripheral meson production, cuts are applied on the missing momentum (pz , pt) $\leq$ (0.1, 0.05).

A preliminary analysis for identifying $\phi\eta$ in the reaction $\gamma p \rightarrow pK^+K^-\eta$ was performed. Events with 3 charged particles consistent with a $proton,\ K^+\ and\ K^-$ were selected from the data. The beam photon was identified via the procedures mentioned above. Figure 9 shows the K^+K^- invariant mass without any missing particle selection. The ϕ meson is clearly observed at the low mass end of the spectrum. The missing mass of the reaction $\gamma p \rightarrow pK^+K^-[X]$ is shown in Figure 10. A clear π^0 signal is observed. An enhancement in the η mass range is also observed. Figure 11 shows the missing mass after an additional cut on the invariant mass of the K^+K^- to select ϕ meson in the event is applied. Peaks for π^0, η and possibly ω meson are visible. These events will be further analysed to observe and isolate possible resonances.

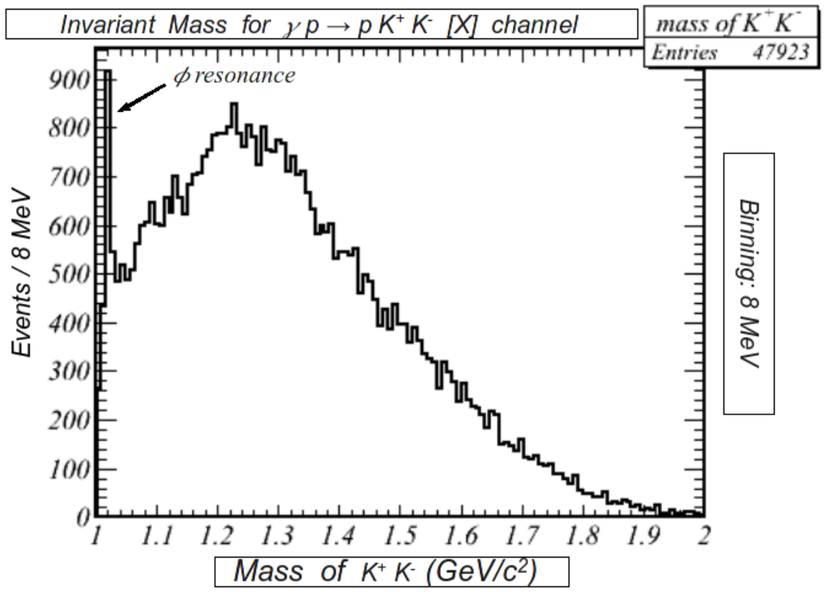

Figure 9: Reconstructed Invariant Mass for K^+K^- from 8% of the data. Peak for the ϕ meson is visible.

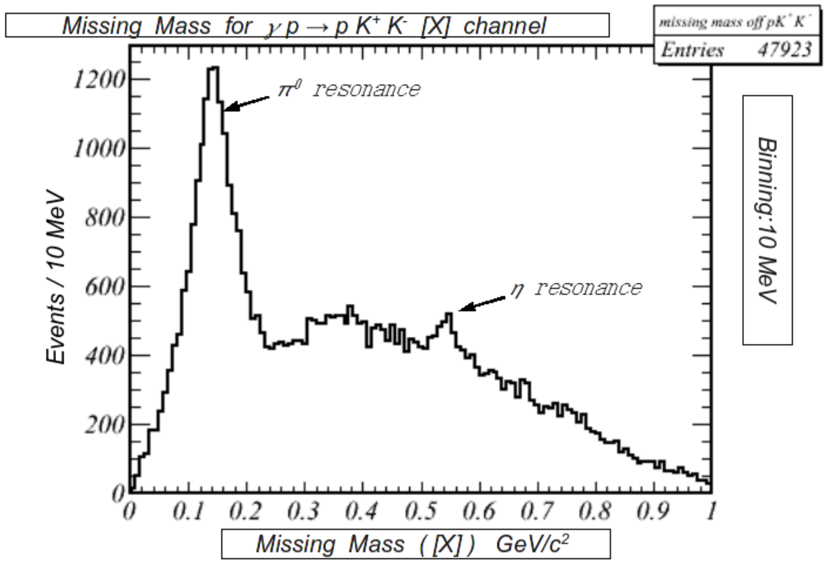

Figure 10: Missing mass using Energy-momentum conservation for final state PK^+K^-. Peaks for π^0 & η are visible.

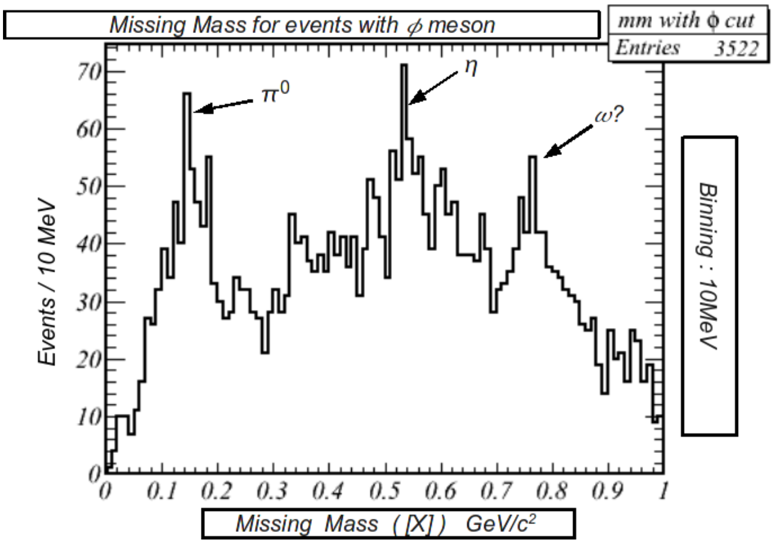

Figure 11: Missing Mass for events where K^+K^- in the event are identified as ϕ's. Peaks for π^0 & ϕ are quite visible whereas another peak that might be possibly ω is visible too. These events will be further analysed for resonances.

References

[1] P. Eugenio, C. Salgado, D. Weygand [CLAS Collaboration], Proposal for g12, E-04-005,(2003).

[2] T. Barnes, N. Black and P. R. Page, Phys. Rev. D **68**, 054014 (2003) [arXiv:nucl-th/0208072].

[3] H. Fritzsch and M. Gell-Mann, eConf **C720906V2**, 135 (1972) [arXiv:hep-ph/0208010].

[4] M. Gell-Mann, Phys. Rev. **125**, 1067 (1962).

[5] M. Y. Han and Y. Nambu, Phys. Rev. **139**, B1006 (1965).

[6] R. P. Feynman, Phys. Rev. Lett. **24**, 1415 (1969).

[7] R. Gupta, Introduction to lattice qcd, (1998).

[8] C. T. H. Davies, Lattice QCD 2007, (2007) [arXiv:hep-ph/0807.1402v1].

[9] H. Yukawa, Proc. Physico-Math. Soc. **17**, Part I (1935).

[10] N. Isgur and J. E. Paton, Phys. Rev. D **31**, 2910 (1985).

[11] T. Barnes, F. E. Close and E. S. Swanson, Phys. Rev. D **52**, 5242 (1995) [arXiv:hep-ph/9501405].

[12] S. Godfrey and J. Napolitano, Rev. Mod. Phys. **71**, 1411 (1999) [arXiv:hep-ph/9811410].

[13] T. Barnes, Acta Phys. Polon. B **31**, 2545 (2000) [arXiv:hep-ph/0007296].

[14] T. Barnes, arXiv:nucl-th/0303032.

[15] F. E. Close and P. R. Page, Phys. Rev. D **52**, 1706 (1995) [arXiv:hep-ph/9412301].

[16] A. P. Szczepaniak and M. Swat, Phys. Lett. B **516**, 72 (2001) [arXiv:hep-ph/0105329].

[17] J. Busenitz *et al.* Phys. Rev. D **40**, 1 (1989)

[18] W. M. Yao *et al.* [Particle Data Group], J. Phys. G **33**, 1 (2006)

[19] J. M. Link *et al.* [FOCUS Collaboration], Phys. Lett. B **545**, 50 (2002) [arXiv:hep-ex/0208027].

[20] G. Ding *et al.* [Babar Collaboration], Physics letters B,**390**(2007)

[21] D. Aston *et al.* [SLAC Collaboration], Physics letters B,**573**(1988)

[22] B. Aubert *et al.* [BaBar Collaboration], Phys. Rev. D **77**, 092002 (2008) [arXiv:hep-ex/0710.4451].

[23] S. I. Bityukov *et. al* Phys. Lett. B **383**, (1987).

[24] B. A. Mecking *et al.* [CLAS Collaboration] NIM A 503 3, **513** (2003).